Molecular BioSystems

Cite this: *Mol. BioSyst.*, 2012, **8**, 1730–1741

www.rsc.org/molecularbiosystems

PAPER

Proteomic analysis of a drosophila IBMPFD model reveals potential pathogenic mechanisms†

Hsin-Tzu Chan,‡[a] Tian-Ren Lee,‡[a] Shun-Hong Huang,[a] Hsiao-Yun Lee,[a] Tzu-kang Sang,[b] Hong-Lin Chan*[a] and Ping-Chiang Lyu*[a]

Received 30th January 2012, Accepted 12th March 2012
DOI: 10.1039/c2mb25037c

IBMPFD, *I*nclusion *b*ody *m*yopathy associated with *P*aget's disease of bone and *f*rontotemporal *d*ementia, is a hereditary degenerative disorder due to single missense mutations in VCP (Valosin-Containing Protein). The mechanisms of how mutations of VCP lead to IBMPFD remain mysterious. Here we utilize two-dimensional difference gel electrophoresis (2D-DIGE) combined with mass spectrometry to study the IBMPFD disorder at the protein level. With this set-up, we are able to employ comparative proteomics to analyze IBMPFD disease using *Drosophila melanogaster* as our disease model organism. Head proteome of transgenic *D. melanogaster* expressing wild type VCP is compared, respectively, with the head proteome of transgenic mutant type VCPs that correspond to human IBMPFD disease alleles ($TER94^{A229E}$, $TER94^{R188Q}$, and $TER94^{R152H}$). Of all the proteins identified, a significant fraction of proteins altered in $TER94^{A229E}$ and $TER94^{R188Q}$ mutants belong to the same functional categories, *i.e.* apoptosis and metabolism. Among these, Drosophila transferrin is observed to be significantly up-regulated in mutant flies expressing $TER94^{A229E}$. A knock-down experiment suggests that fly transferrin might be a potential modifier in IBMPFD disease. The molecular analysis of IBMPFD disease may benefit from the proteomics approach which combines the advantages of high throughput analysis and the focus on protein levels.

Introduction

Hereditary inclusion body myopathy (IBM) associated with Paget's disease of bone (PDB) and frontotemporal dementia (FTD), also known as IBMPFD, is a hereditary, autosomal dominant and ultimately lethal multi-system disorder.[1–4] IBMPFD features three variably penetrating phenotypes including adult-onset proximal and distal muscle weakness, osteolytic lesions consistent with early-onset PDB, and FTD manifested by prominent language and behavioral dysfunction.[4,5] Myopathy is the presenting symptom in approximately 90% of the affected individuals, leading to loss of walking ability and even death by complications of respiratory and cardiac failure.[3,5] About 50% of the IBMPFD individuals develop Paget's disease of bone which is characterized by abnormal rates of bone growth and can result in bone pain, enlargement and fractures.[1,6–8] Approximately one-third of the IBMPFD patients are associated with frontotemporal dementia, which is similar to the conditions suffered by patients with Alzheimer's, Parkinson's and Huntington's diseases.[9,10] People with IBMPFD usually live into their fifties or sixties.[1] Unfortunately, there are no known cures or treatments for IBMPFD patients.

IBMPFD is caused by missense mutations in the gene encoding VCP (valosin-containing protein, also known as p97), which is a member of the AAA-ATPase (ATPases associated with a variety of activities) superfamily.[1,4,11–14] VCP is characterized by a tripartite structure comprising an N-terminal domain which is involved in ubiquitin/cofactor binding, and two AAA domains (D1 and D2) that are responsible for the formation of stable hexamers and ATPase activity, respectively (ESI†, Fig. S1A).[15–17] VCP assembles into a functional homohexamer with D1 and D2-domains stacked on top of each other. The two stacked rings form a pore in the center, and the two domains are surrounded by the N-domains (ESI†, Fig. S1B).[15–17] Up to date, thirteen unique missense mutations in VCP have been reported to associate with IBMPFD in which reside, within the N domain, loop 1 or D1 domain (ESI†, Fig. S2).[1,2,4]

VCP is ubiquitous within the cell, accounting for more than 1% of the total cellular proteins. VCP has been implicated in a variety of cellular activities, including cell cycle control, membrane fusion, ERAD degradation and apoptosis.[17] It is conjectured that because of the importance of VCP and

[a] *Institute of Bioinformatics and Structural Biology & Department of Medical Sciences, National Tsing Hua University, No.101, Kuang-Fu Rd. Sec.2, Hsinchu, 30013, Taiwan. E-mail: hlchan@life.nthu.edu.tw, pclyu@mx.nthu.edu.tw*
[b] *Institute of Biotechnology & Department of Life Sciences, National Tsing Hua University, Hsinchu, Taiwan*
† Electronic supplementary information (ESI) available. See DOI: 10.1039/c2mb25037c
‡ These authors contributed equally to this work.

the multiple roles it plays, it is highly conserved throughout evolution across species with orthologues in archaebacteria (VAT), yeast (CDC48), *Drosophila* (TER94), *Xenopus* (p97), and plants and mammals (VCP).[12,18] Most importantly, VCP disease mutation sites are highly conserved across different species (ESI†, Fig. S3).[17,19,20] How VCP mutations lead to IBMPFD has attracted a great deal of attention from researchers in different fields and still remains to be elucidated.

Drosophila melanogaster has been a powerful and most commonly utilized model organism for the study of various human diseases such as Alzheimer's, Parkinson's, Huntington's diseases, *etc*.[21,22] *Drosophila* transgenic strains have been developed to help scientists immensely to advance the understanding of many complex disorders. In this study, the GAL4/UAS (upstream activating sequence) system is applied to overexpress *Drosophila* VCP homolog TER94 mutants that correspond to human IBMPFD disease alleles in a tissue specific fashion. In this system, TER94 transgene is placed under the control of the yeast transcriptional activator GAL4. In the absence of GAL4, the transgene is inactive. When flies express GAL4 in a specific tissue or cell type, protein TER94 is translated only in the tissues that have GAL4 (ESI†, Fig. S4). The fly model serves as a useful model for IBMPFD study because it showed that overexpression of TER94 mutants had caused severe phenotypes including neurodegenerative, memory impairment, and defect in flight performances, which seemed reminiscent of the multi-degenerative phenotypes observed in IBMPFD patients.[23] In addition, two-dimensional difference gel electrophoresis (2D-DIGE) (ESI†, Fig. S5) combined with mass spectrometry were utilized to study IBMPFD at the protein level. With this set up, comparative proteomics is employed for the analysis of IBMPFD disease using *Drosophila melanogaster*

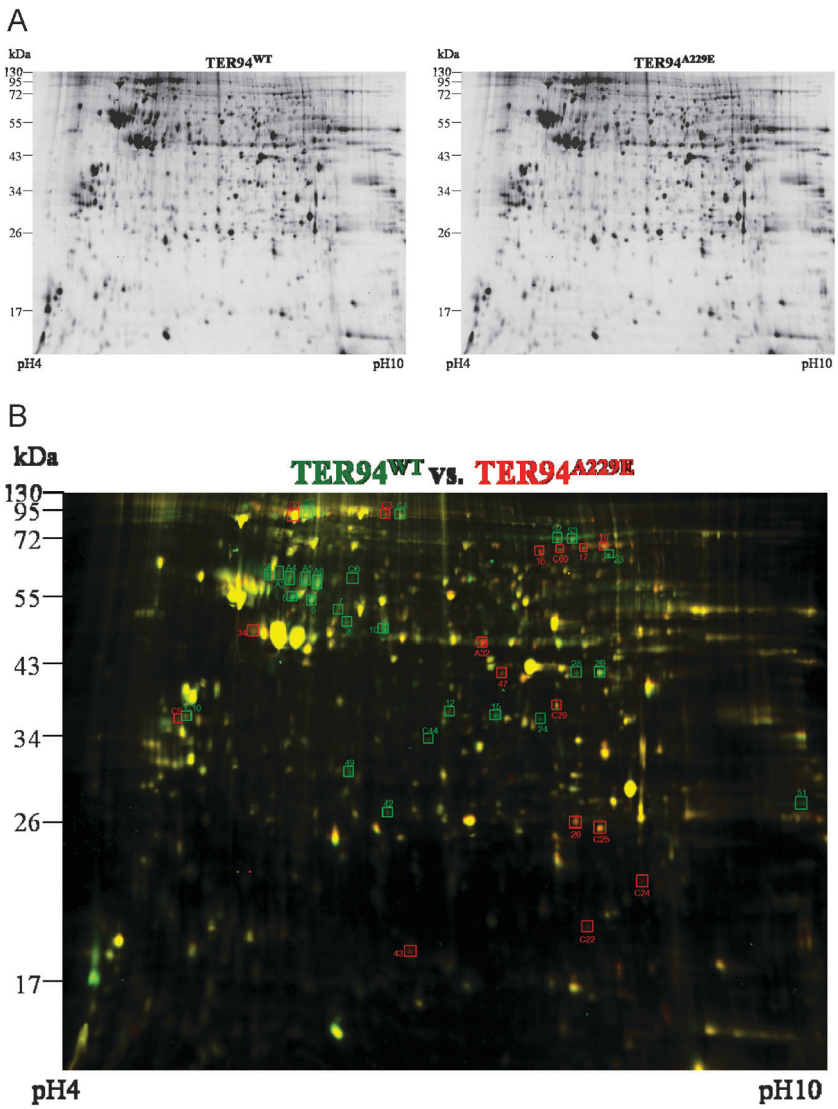

Fig. 1 Head proteome maps of TER94^{WT} and TER94^{A229E} fly strains. (A) Head proteins from TER94^{WT} and TER94^{A229E} fly strains were labeled with Cy3 and Cy5, respectively, and separated by IEF in the first dimension using 24 cm IPG strips (pH 4–10), then by size (13–130 kDa) in the second dimension. Representative images were scanned with an Ettan^{TM} DIGE Imager. (B) 2D images of head proteomes from flies expressing wild-type TER94 and mutant TER94^{A229E} are superimposed. Green spots represent an up-regulation of protein expression in flies expressing wild-type TER94. Red spots represent an up-regulation of protein expression in flies expressing TER94^{A229E}. Yellow spots represent an equal amount of protein expression in both fly strains. Significant differential proteins are marked and numbered, and their corresponding IDs are shown in Table 1.

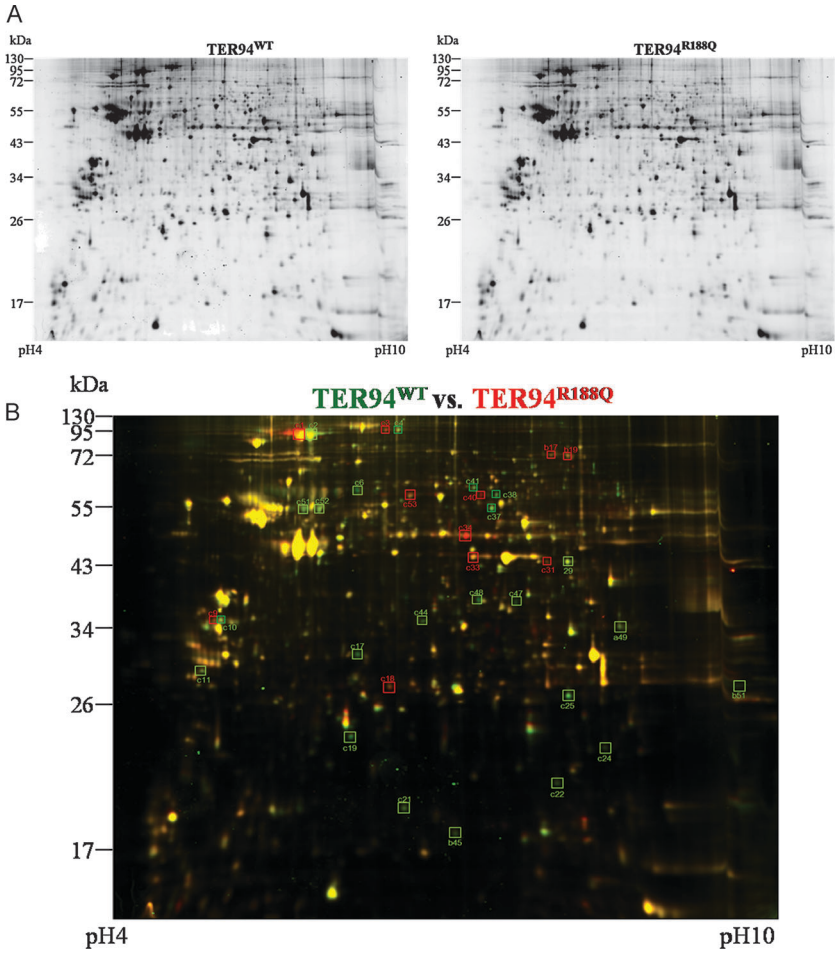

Fig. 2 Head proteome maps of TER94^{WT} and TER94^{R188Q} fly strains. (A) Head proteins from TER94^{WT} and TER94^{R188Q} fly strains were labeled with Cy3 and Cy5, respectively, and separated by IEF in the first dimension using 24 cm IPG strips (pH 4–10), then by size (13–130 kDa) in the second dimension. Representative images were scanned with an Ettan^{TM} DIGE Imager. (B) 2D images of head proteomes from flies expressing wild-type TER94 and mutant TER94^{R188Q} are superimposed. Green spots represent an up-regulation of protein expression in flies expressing wild-type TER94. Red spots represent an up-regulation of protein expression in flies expressing TER94^{R188Q}. Yellow spots represent an equal amount of protein expression in both fly strains. Significant differential proteins are marked and numbered, and their corresponding IDs are shown in Table 3.

as our disease model organism. Head proteome of transgenic *D. melanogaster* expressing TER94/VCP-WT is, respectively, compared with the head proteome of transgenic *D. melanogaster* expressing TER94/VCP mutants that correspond to human IBMPFD disease alleles (TER94^{A229E}, TER94^{R188Q} and TER94^{R152H}). Combining both tissue-specific and proteomics approaches, we are able to elucidate the cellular consequences of TER94/VCP mutations at the protein level.

Materials and methods

Drosophila strains and genetic crosses

All the fly strains used in this report are in wild-type w1118 genetic background. A fly strain with a UAS-TER94^{WT} responder line was mated to a fly strain carrying a GMR-GAL4 driver to drive the expression of TER94^{WT} in progenies. Flies were reared in glass vials containing culture medium (0.9% agar medium containing 10.5% dextrose, 5% cornmeal, 2.6% baker's yeast, and 0.23% tegosept, to which active yeast is added). Flies were raised under a 12 hour light–12 hour dark cycle in a temperature and humidity controlled incubator (25 °C and 60–70% humidity).

Protein lysate preparation

The entire head proteins were extracted for head proteome comparisons. Flies (150 male flies and 150 female flies) were collected into centrifuge tubes (50 ml). Liquid nitrogen was then added into the tubes before shaking vigorously to separate heads from bodies and extremities. Fly heads were isolated using pre-chilled size exclusion sieves. The top sieve (Tyler equivalent 25 mesh#, 0.71 mm^2) allowed the heads to pass to the bottom sieve (Tyler equivalent 40 mesh#, 0.42 mm^2), which separated the extremities from the heads. The heads were collected and pulverized in liquid nitrogen with a pre-chilled mortar and pestle and then transferred to a micro-centrifuge tube. All samples were precipitated and extracted by methanol/chloroform strategy according to the protocol described previously with slight modifications.[24] Samples were suspended in NHS-lysis buffer consisting of 7 M urea, 2 M thiourea, and 4% (w/v) CHAPS followed by addition of methanol,

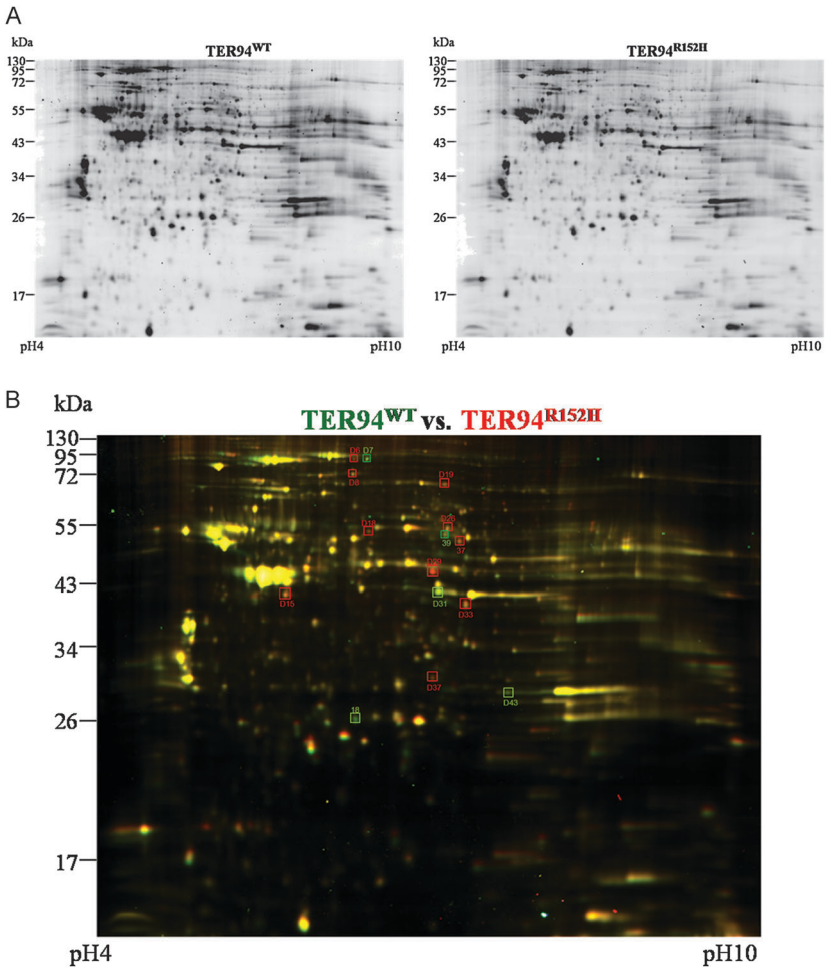

Fig. 3 Head proteome maps of TER94^{WT} and TER94^{R152H} fly strains. (A) Head proteins from TER94^{WT} and TER94^{R152H} fly strains were labeled with Cy3 and Cy5, respectively, and separated by IEF in the first dimension using 24 cm IPG strips (pH 4–10), then by size (13–130 kDa) in the second dimension. Representative images were scanned with an Ettan^{TM} DIGE Imager. (B) 2D images of head proteomes from flies expressing wild-type TER94 and mutant TER94^{R152H} are superimposed. Green spots represent an up-regulation of protein expression in flies expressing wild-type TER94. Red spots represent an up-regulation of protein expression in flies expressing TER94^{R152H}. Yellow spots represent an equal amount of protein expression in both fly strains. Significant differential proteins are marked and numbered, and their corresponding IDs are shown in Table 4.

chloroform, and ddH_2O. Prior to adding each solution, samples were well-vortexed and centrifuged at 14 000 rpm for five minutes at room temperature. Top aqueous layers were discarded in all samples. Subsequently, samples were washed with methanol and centrifuged again at 14 000 rpm for five minutes at room temperature. Finally, top methanol layers were removed as much as possible, and the samples were vacuum dried.

Lysates were homogenized by injecting through a 26-gauge needle, and the insoluble substances were removed by centrifugation at 14 000 rpm at 4 °C for thirty minutes. Protein concentration was determined by a Bradford protein assay kit (BioRad).

Two-dimensional differential gel electrophoresis (2D-DIGE)

Protein samples were each labeled with 4 pmol per μg of CyDye^{TM} DIGE fluorescent minimal dyes, Cy2, Cy3, and Cy5 in the dark for thirty minutes according to the protocol described previously.[25,26] After labeling, 100 mM L-lysine was added to terminate the reaction between the dye and the OH groups on lysines. Samples were mixed in one tube and equilibrated in 1.3 M of DTT for fifteen minutes followed by fifteen minutes of equilibration in the ampholines/Pharmalyte mix. IPG buffer, pH 3–10 nonlinear (2% (v/v), GE Healthcare) was added and the final volume was adjusted to 450 μl with 2D-lysis buffer for rehydration. Immobiline DryStrips (pH 3–10 non-linear, 24 cm) with samples loaded were rehydrated in a reswelling tray with mineral oil placed on top of the sample to prevent evaporation. The immobilized IPG strips were rehydrated for 12 hours according to the manufacturer's instructions (passive rehydration method).

Isoelectric focusing was performed with Multiphor II apparatus (GE Healthcare) for a total of 62.5 kV h at 20 °C. IPG strips were reduced for 15 minutes with 65 mM dithiothreitol in equilibration buffer (6 M urea, 30% (v/v) glycerol, 50 mM Tris–HCl pH 6.8, 2% (w/v) SDS) followed by 15 minutes of alkylation in the same buffer containing 240 mM iodoacetamide. For the second dimension, the equilibrated strips were loaded onto a 24 cm 12.5% SDS-polyacrylamide gel. The IPG strips-loaded polyacrylamide gels were run in an Ettan Twelve gel tank (GE Healthcare) at 4 Watt per gel at 10 °C until the dye front had completely run off to the bottom of the gels.

Table 1 List of up-regulated and down-regulated proteins expressed in $TER94^{WT}$ fly strain in comparison to $TER94^{A229E}$ fly strains

Spot no.	Protein name	M_W	MASCOT score[a]	p*I*	Coverage (%)	Matched peptide sequences
Up-regulated in TER94WT fly strain in comparison to TER94A229E fly strains						
A3	Drosocrystallin	55 248	136/60	5.54	32	DSLTGDDKR; LDEQQQQR
A4	Drosocrystallin	55 248	123/60	5.54	28	DSLTGDDKR; LDEQQQQR
A5	Drosocrystallin	55 248	101/60	5.54	15	GQYSLIEPDGTR; DSLTGDDKR
A6	Drosocrystallin	55 248	120/60	5.54	23	LDEQQQQR; AGAALSWSNGR
C2	Transitional endoplasmic reticulum ATPase TER94	89 545	127/48	5.21	19	GILMYGPPGTGK; EIDIGIPDATGR
C4	Iron regulatory protein 1B (SD12606p)	99 031	145/60	5.6	17	EEGTPLVLVVGK; VSVSDMPEDFK
C6	Drosocrystallin	55 248	78/60	5.54	13	DSLTGDDKR; LDEQQQQR
C44	CG32029-PA (RE57183p)	30 860	70/60	5.97	22	GSYSVVDSDGFIR; GSYSVVDSDGFIRTVK
4	Drosocrystallin	55 248	123/60	5.54	41	LPGSTTTSSSR; DSLTGDDKR
5	Cuticular protein 72Ec CG4784-PA	50 593	169/60	5.4	36	AELSAMLADR; QDLRQDQSR
6	Cuticular protein 72Ec CG4784-PA	50 593	98/60	5.4	23	QDLRQDQSR; VRAELSAMLADR
7	Protein henna	52 084	155/48	5.57	31	MYQRQVSFDKPTR; YFADIAYNYK
8	Cuticular protein 72Ec CG4784-PA	50 593	96/60	5.4	28	VRAELSAMLADR; QDQSRNQESLR
10	Cuticular protein 72Ec CG4784-PA	50 593	117/60	5.4	28	VRAELSAMLADR; QISSDRDGDDLR
12-1	GTP cyclohydrolase 1	35 804	53/48	6.16	16	EALLPDMARSYR; TVTSTMLGVFR
12-2	Eukaryotic translation initiation factor 4E	29 320	70/48	5.83	33	MQSDFHRMK; MQSDFHR
15	GTP cyclohydrolase 1	35 804	78/48	6.16	16	EALLPDMARSYR; TVTSTMLGVFR
23	Pro-phenol oxidase A1	79 441	183/60	6.14	33	QEASVIGESGAR; NQALNLEEQR
24	GTP cyclohydrolase 1	35 804	76/48	6.16	16	AAKAMLYFTK; TVTSTMLGVFR
28	Guanine nucleotide-binding protein subunit β-2	39 109	76/48	6.3	16	LYDEINGMIQK; LWDVREEGHK
29	Guanine nucleotide-binding protein subunit β-2	39 109	82/48	6.3	23	LYDEINGMIQK; MPKIDPETQK
42	Triosephosphate isomerase	26 894	92/48	6	29	QWLSDNISK; GAFTGEISPAMLK
49	Sepia CG6781-PA (RH04924p)	28 566	139/60	5.58	43	FPQLTLWLERMK; GSPMPDVPEDGILR
51	Pigment cell dehydrogenase reductase	28 455	74/60	8.83	19	LRAAHPTQSVMIIK; AAHPTQSVMIIK

Spot no.	Protein name	M_W	MASCOT score[a]	p*I*	Coverage (%)	Matched peptide sequences
Down-regulated in TER94WT fly strain in comparison to TER94A229E fly strains						
A32	Isocitrate dehydrogenase CG7176-PB, isoform B	50 799	101/66	7.59	19	QPHLSQAVFR; LIDDMVAYAMK
C1	Transitional endoplasmic reticulum ATPase TER94	89 545	144/48	5.21	22	EKMDLIDLEDDK; IVSQLLTLMDGMK
C3	Iron regulatory protein 1B (SD12606p)	99 031	137/60	5.6	15	EEGTPLVLVVGK; RPPFFEGMTR
C24	CG10233-PA, isoform A (GH04877p)	23 010	87/60	6.62	27	ADGMKYEGEFR; MAMDDYDDDMSSVGVTTA
C25	Superoxide dismutase, CG8905-PA	24 815	83/66	7.74	31	LIQLAPALR; EIMELHHQK
C29	CG6084-PA, isoform A (LD06393p)	36 185	114/60	6.21	36	EVPIIGLGTWGSPK; LWNTFHRPDLVK
C60	Transferrin CG6186-PA	72 964	104/60	6.69	15	VSSSDDGEVQIVPASELEK; SDTTSVEQETVK
16	Pro-phenol oxidase A1	79 441	194/60	6.14	31	VEVPEGYFPK; ANTLLTYWQK
17	Transferrin precursor/transferrin CG6186-PA	72 963	168/60	6.89	24	NVGYKIPITK; SDTTSVEQETVK
19	Transferrin CG6186-PA	72 964	145/60	6.69	22	SDTTSVEQETVK; DSPIRTLQQLR
34	Actin	42 174	127/48	5.3	37	HQGVMVGMGQK; QEYDESGPGIVHR
43	Twinstar CG4254-PA/cofilin/actindepolymerizing factor homolog	17 428	90/48	6.74	33	TTYEEIK; MLYSSSFDALKK
47	Pyruvate dehydrogenase	44 320	149/60	7.57	29	HNDVVQTMAQGVIEMK; ALSDEANELLPIFNK

[a] The scores means ($-10\text{Log}(P)$, where P is the probability/threshold score with p-value = 0.05). Identified proteins with a score, $-10\text{Log}(P)$, greater than threshold scores demonstrate the identification of this protein is significant ($p < 0.05$).

Image analysis

Gel images were scanned with an Ettan™ DIGE Imager and analyzed with DeCyder™ v7.0 software according to the protocols provided by GE Healthcare. Samples that had been previously labeled with different cyanine reactive dyes responded distinctively to a specific wavelength under appropriate excitation and emission conditions. Protein spots were matched automatically using the DIA (Difference In-gel Analysis) module. The DIA module processes a triplet of images from a single gel. Therefore, three images from a single gel can be co-detected. Spot intensities were normalized to make the total density in each gel image equal, and analysis was performed using quantitative and qualitative modes.

In-gel digestion and peptide extraction

Spots of interest from the gels were excised and washed in wash buffer (10 mM NH_4HCO_3, 50% (v/v) ACN) for 15 minutes. The solution was then removed, and ACN was added to cover the gel pieces. Gel pieces were rehydrated again with 20 mM NH_4HCO_3 for 5 minutes. ACN was added for

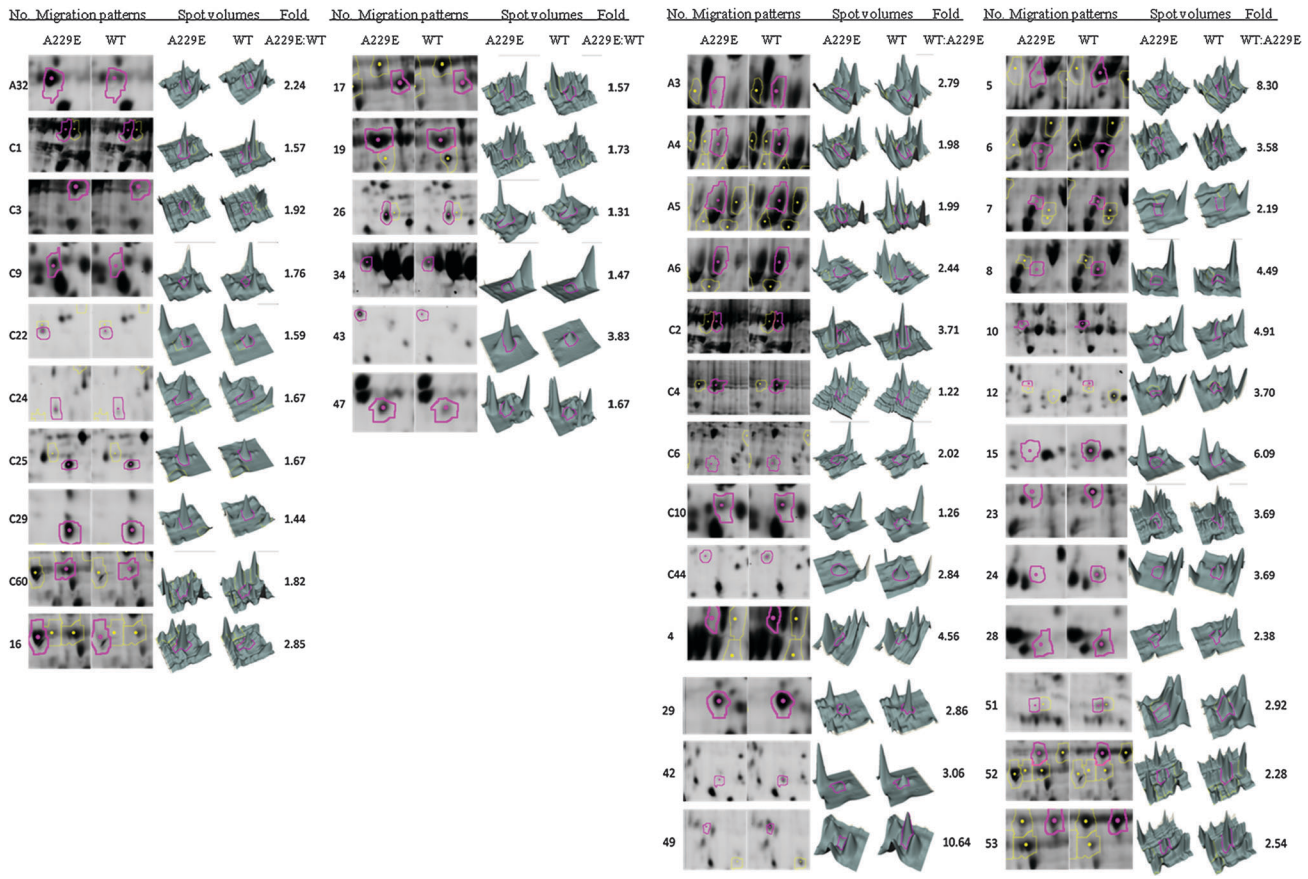

Fig. 4 Spot volume of altered expressed head proteins in between TER94^{WT} and TER94^{A229E} fly strains. Selected area of two-dimensional gels and corresponding spot intensities for selected spots identified in TER94^{WT} and TER94^{A229E} fly strains are shown. Protein spot migration patterns were detected in 2D-DIGE gels using an EttanTM DIGE Imager. Image pairs and detection of protein spots with relative spot volumes were achieved using DeCyder software. Proteins with relatively higher expression levels in flies expressing wild-type TER94 are shown.

another 15 minutes of sonication. These steps were repeated until the gel pieces were well-washed. Finally, gel pieces were dried in a SpeedVac for 20 minutes. After drying, freshly prepared enzyme solution (20 ng per μl of trypsin, in 10 mM NH_4HCO_3) was added to the tubes to cover the gel, and was incubated at 24 °C for 60 minutes. An additional 3 μl of 10 mM NH_4HCO_3 was added to keep the gel wet overnight. The gel pieces were incubated overnight at 37 °C for trypsin digestions.

Trypsin-digested pieces were extracted with 50% (v/v) ACN with 1% (v/v) TFA. Gel extraction was repeated 4 times, and the supernatants were pooled. The supernatants were vacuum-dried, and the dry residues were dissolved in 1 μl of 1% (v/v) TFA. Subsequently, 1 μl of this solution was directly spotted on the MALDI-TOF anchorchip target plate. After the samples were dried, 1 μl of α-cyano-4-hydroxycinnamic acid (CHCA) MALDI-MS matrix was covered on the samples and allowed to dry before the measurement in MALDI-TOF.

Protein identification and database search

MALDI-TOF MS with generated peptide mass fingerprints were searched against databases for protein identifications. Peptide mass fingerprints were obtained by an Autoflex III mass spectrometer (Bruker Daltonics). The spectrometer was internally calibrated using trypsin autolysis peaks at m/z 842.51 and m/z 2211.10. Peaks of the peptide mass fingerprint in the mass range m/z 800–3000 were searched against databases using Mascot software v2.2.04. The parameters used for searching were: *D. Melanogaster*; tryptic digest with a maximum of 1 missed cleavage; carbamidomethylation of cysteines, partial protein N-terminal acetylation, partial methionine oxidation and partial modification of glutamine to pyroglutamate and a mass tolerance of 100 ppm. Proteins were identified based on the significance of the MASCOT Mowse scores ($p < 0.05$), spectrum annotations, molecular weight and the pI values.

Results and discussions

Proteome comparisons between wild type and disease-linked mutant TER94 reveal alteration of proteins involved in energy production

Head proteomes of *Drosophila* expressing mutant TER94 (TER94^{A229E}, TER94^{R152H} and TER94^{R188Q}) were first compared with the head proteome of *Drosophila* expressing wild-type TER94 (TER94^{WT}) (Fig. 1, 2 and 3), in which TER94^{A229E} strain has been reported to be the most severely degenerated phenotype compared with the other two mutant strains (TER94^{R152H} and TER94^{R188Q}).[23] When 2D-DIGE head proteome images of *Drosophila* TER94^{WT} and TER94^{A229E}

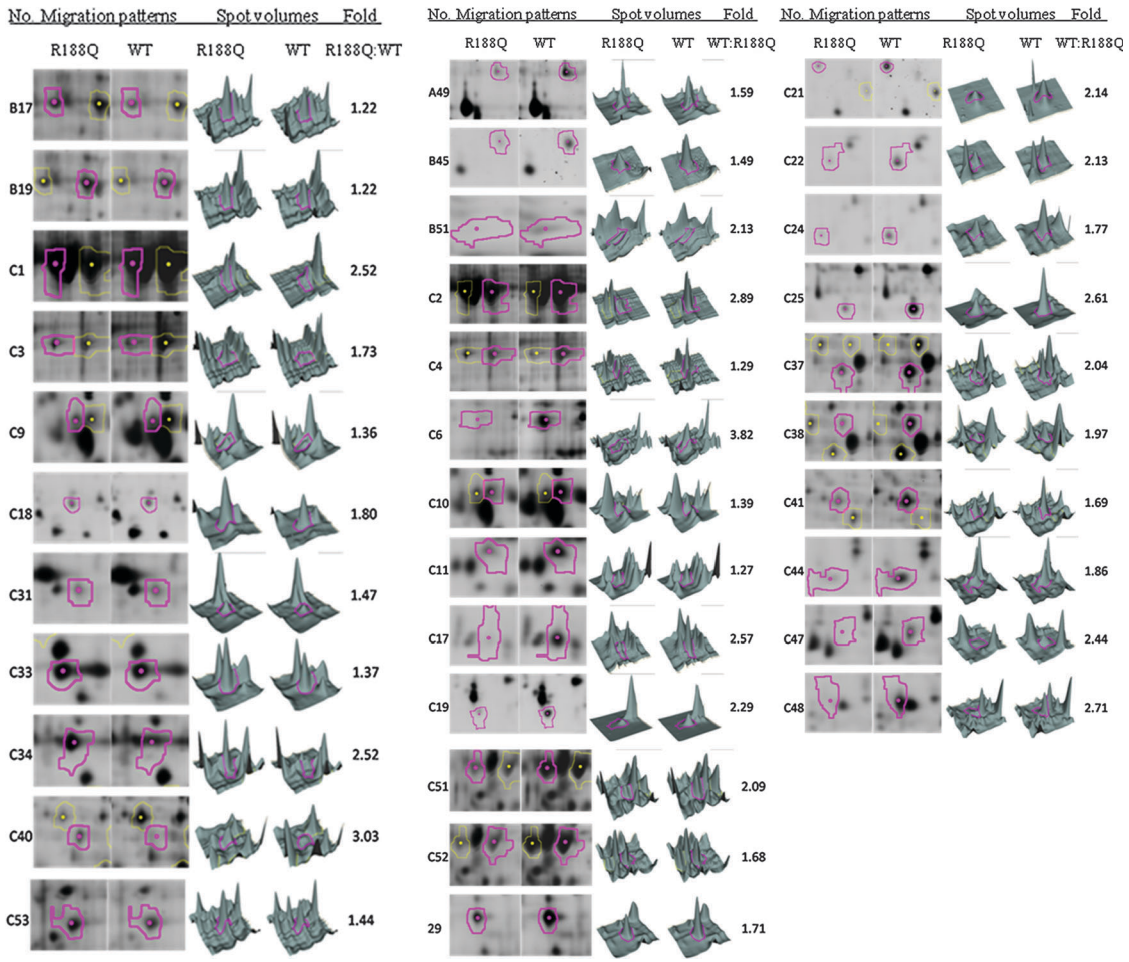

Fig. 5 Spot volume of altered expressed head proteins in between $TER94^{WT}$ and $TER94^{R188Q}$ fly strains. Selected area of two-dimensional gels and corresponding spot intensities for selected spots identified in $TER94^{WT}$ and $TER94^{R188Q}$ fly strains are shown. Protein spot migration patterns were detected in 2D-DIGE gels using an EttanTM DIGE Imager. Image pairs and detection of protein spots with relative spot volumes were achieved using DeCyder software. Proteins with relatively higher expression levels in flies expressing wild-type TER94 are shown.

strains are superimposed, red spots represent an up-regulation of protein expression in flies expressing $TER94^{A229E}$, green spots represent a down-regulation of protein expression in flies expressing $TER94^{A229E}$, and yellow spots represent an equal amount of protein expression in both fly strains (Fig. 1). A total of forty-three differential spots were extracted for identification. These proteins, twenty-four from $TER94^{WT}$ fly strain and thirteen from $TER94^{A229E}$ fly strain are up-regulated and listed in Table 1. Additionally, thirty-one and thirteen spots corresponding to the differentially expressed in $TER94^{R188Q}$/$TER94^{WT}$ and in $TER94^{R152H}$/$TER94^{WT}$ were identified, respectively (Fig. 2, Fig. 3, Table 3). Spot volume comparisons of the differential protein spots using the Differential in-gel Analysis (DIA) DeCyder^{TM} model are shown in Fig. 4–6.

Differentially expressed proteins between $TER94^{WT}$ fly strain and $TER94^{A229E}$ fly strain have diverse functional characteristics, including the structural constituent of eye, protein degradation, metabolic pathway, cell structure and mobility, cell signaling, genetic information processing, protein transportation, and cellular defense (Table 2). Of all these proteins grouped in functional categories, we first looked at the eye-related proteins because wild-type and mutant flies have distinct eye phenotypes; wild-types have intact eyes whereas mutants have degenerated eyes.[23] Eight distinct spots (A3, A4, A5, A6, C6, 4, 49 and 51) are identified to participate in the structural constituent of eye. Six of these proteins (A3, A4, A5, A6, C6, and 4) are drosocrystallin, a major protein component that participates in the corneal lens formation. Spot 49 is sepia, which participates in the eye pigment biosynthetic process. Spot 51 is a pigment cell dehydrogenase reductase, which is responsible for eye pigmentation. These eye-related proteins are observed to be down-regulated in *Drosophila* expressing mutant TER94 (GMR > $TER94^{A229E}$), which corresponds to the observed phenotype that shows degenerated eye morphology in $TER94^{A229E}$ but not $TER94^{WT}$.[23]

We have previously reported a connection between ATP consumption and IBMPFD in the *Drosophila* model; IBMPFD-linked mutations showed an increase in energy demand and the resulting phenotype could be repressed by boosting energy production. This observation is supported by a report that showed disease-linked VCP mutants exhibiting three fold increase in ATPase activity compared to the wild-type.[27] In our 2D-DIGE proteome, the citric acid cycle (TCA)-related

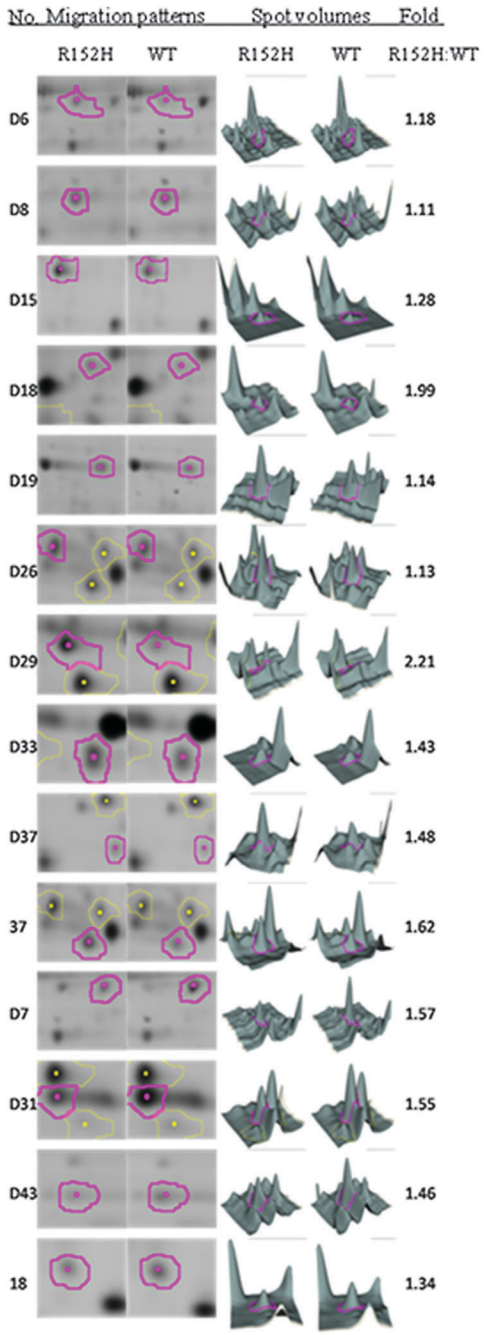

Fig. 6 Spot volume of altered expressed head proteins in between TER94^{WT} and TER94^{R152H} fly strains. Selected area of two-dimensional gels and corresponding spot intensities for selected spots identified in TER94^{WT} and TER94^{R152H} fly strains are shown. Protein spot migration patterns were detected in 2D-DIGE gels using an EttanTM DIGE Imager. Image pairs and detection of protein spots with relative spot volumes were achieved using DeCyder software. Proteins with relatively higher expression levels in flies expressing wild-type TER94 are shown.

proteins such as isocitrate dehydrogenase (spotA32) and pyruvate dehydrogenase are up-regulated in mutant TER94^{A229E} strain. Citric acid cycle generates energy and produces the majority of the ATP in the cell. Therefore, greater abundance of TCA-related proteins observed in TER94^{A229E} strain correlates with our previous finding that flies with mutated TER94 possess higher energy demand.[23] As a consequence, increased production of ATP is needed for cellular energy supply. It is noteworthy that up-regulation of different isoforms of isocitrate dehydrogenase (encoded by Drosophila CG7176) was observed in other disease-linked mutants (Tables 3 and 4), which further supports that energy expenditure may play an essential role in IBMPFD pathogenesis.

Proteins involved in metabolic processes show diversified levels in disease flies

Given the potential change of energy expenditure when expressing a VCP disease mutant, it is perceivable that cells may attempt to balance the energy demands by altering pathways involving in the metabolic processes. Indeed, in our proteome results, alteration of protein levels which has a clear role in metabolic pathway is readily identified. Among these, iron regulatory protein 1B is upregulated in all mutant TER94 (TER94^{A229E}, TER94^{R152H} and TER94^{R188Q}) compared to wild-type TER94. Interestingly, we also identified transferrin as being upregulated in disease flies (C60, 17, and 19 with different post-translational modifications). Transferrin is a blood plasma protein for iron ion delivery. When a transferrin protein is loaded with iron ions, it encounters a transferrin receptor on the membrane surface and is transported into the cell in a vesicle. After transferrin releases its iron ions into the cells, transferrin receptor with its ligand, transported through the endocytic cycle back to the cell surface, ready for another round of iron uptake. A recent study of DiFiglia and colleagues demonstrated that Rab11 correlates with transferrin recycling.[28] Mutant Huntington (Htt) impairs Rab11, which damages vesicle formation. Impairment of vesicle formation delays transferrin-recycling back to the plasma membrane, which could lead to oxidative stress and mitochondrial dysfunction. Therefore, it is suggested that transferrin accumulation observed in our 2D-DIGE result is due to vesicle formation impairment. Actually, knock-down of transferrin in transgenic mutant TER94^{A229E} flies significantly suppresses the phenotype of mutant flies in our recent published report.[23] Although it is not clear whether Drosophila transferrin plays a conserved role in iron transport, this finding suggests that transferrin is an essential protein in IBMPFD development. Importantly, of the protein isoforms identified by 2D-DIGE/MALDI-TOF methods, iron regulatory protein 1B were identified as doublet spots with differing p*I*s by lysine labeling (C3 and C4 in TER94^{A229E} (Fig. 1), C3 and C4 in TER94^{R188Q} (Fig. 2), D6 and D7 in TER94^{R152H} (Fig. 3)). Notably, the more basic spots in these doublets were all shown to be up-regulated in TER94^{WT} compared with mutant strains TER94^{A229E}, TER94^{R188Q}, TER94^{R152H}, whilst the more acid spots in these doublets were all shown to be up-regulated in mutant strains TER94^{A229E}, TER94^{R188Q}, TER94^{R152H} compared with wild type strain TER94^{WT}. A similar observation has been reported by Chan *et al.*[26] and was found to be due to oxidation of the cysteine thiols of these proteins. Such acid shifts provide an explanation for the observed differential labeling by the 2D-DIGE strategy. Accordingly, we proposed that the shifts were caused by post-translational modifications of iron regulatory protein 1B. However, the detailed modifications and mechanisms might need further investigation and validation.

Table 2 List of identified proteins from TER94^{WT} and TER94^{A229E} grouped in functional categories

Protein folding, sorting, and degradation	Signaling protein
C1. Transitional endoplasmic reticulum ATPase	28. Guanine nucleotide-binding protein subunit β2
C2. Transitional endoplasmic reticulum ATPase	29. Guanine nucleotide-binding protein subunit β2
Metabolic pathway	Genetic info. processing; replication and repair
A32. Isocitrate dehydrogenase CG7176-PB	12-2. Eukaryotic translation initiation factor 4E
C3. Iron regulatory protein 1B	
C4. Iron regulatory protein 1B	Transport protein
C29. CG6084-PA, isoform A (LD06393p)	C60. Transferrin CG6186-PA
7. Protein henna	17. Transferrin precursor
12-1. GTP cyclohydrolase 1	19. Transferrin CG6186-PA
15. GTP cyclohydrolase 1	
16. Pro-phenol oxidase A1	Cellular defense
23. Pro-phenol oxidase A1	C25. Superoxide dismutase
24. GTP cyclohydrolase 1	
42. Triosephosphate isomerase	Others
47. Pyruvate dehydrogenase	C24. CG10233-PA, isoform A
	C44. CG32029-PA
Structural constituent of eye	5. Cuticular protein 72Ec CG4784-PA
A3. Drosocrystallin	6. Cuticular protein 72Ec CG4784-PA
A4. Drosocrystallin	8. Cuticular protein 72Ec CG4784-PA
A5. Drosocrystallin	10. Cuticular protein 72Ec CG4784-PA
A6. Drosocrystallin	
C6. Drosocrystallin	
4. Drosocrystallin	
49. Sepia CG6781-PA (RH04924p)	
51. Pigment cell dehydrogenase reductase	
Cell structure and mobility protein	
34. Actin	
43. Twinstar/Cofilin/actin-depolymerizing factor	

Actin and its regulator response to disease-linked mutant TER94

Actin dynamics in cells is a major ATP-using process.[29] It has been reported that reduction in actin dynamics is a result of ATP depletion.[30] Cells that are depleted of ATP shift towards a less dynamic, ADP-actin-rich structure, which favors the production of actin aggregates.[31] Interestingly, in our proteomic result, cytoskeleton-related proteins such as actin (spot34) and cofilin (spot43) are observed to be up-regulated in flies expressing mutant TER94^{A229E}. Actin has been reported to participate in aging and apoptosis.[32–38] Decreased actin dynamics results in activation of the Ras2/cAMP/PKA signaling pathway, which is amplified by a positive regulation loop that promotes actin aggregation. This in turn causes mitochondrial changes and triggers ROS production followed by apoptosis.[32] Depletion, mutation or oxidative modification of VCP results in decreased cellular activity of VCP. This in turn causes ER stress and oxidative stress that triggers the mitochondrial production of reactive oxygen species (ROS) which then activates caspase activities and triggers apoptotic cell death. TER94/VCP is known to participate in various imperative cellular processes, including apoptosis (Fig. 7).[23,39] Therefore, the control of actin dynamics is necessary for vital mitochondrial function and integrity. A possible explanation for the up-regulation of actin observed in the mutant TER94^{A229E} proteome is probably due to actin aggregation which is caused by reduced actin dynamics.

A potential role of ROS in fly IBMPFD model

ROS are highly reactive molecules that contain oxygen ions and peroxides. Increased ROS levels can result in oxidative stress which triggers apoptosis. Cells defend themselves against ROS damage through the use of antioxidant enzyme molecules, such as catalase, glutathione and superoxide dismutase. In our 2D gel, superoxide dismutase is observed to be up-regulated in mutant TER94^{A229E} flies. A possible explanation for this phenomenon is that mutation of TER94 triggers the mitochondrial production of ROS, which promotes caspase activities and activates apoptotic cell death (Fig. 4). Cells need to produce an increased amount of SOD to defend themselves against ROS damage and protect themselves from going into apoptosis. A similar finding was reported from a study of Ueffing.[40] When CDC48/VCP is mutated in yeast cells, accumulation of glutathione is found in mitochondrial extracts which also hints to an increased oxidative stress in yeast cells expressing mutant CDC48. SOD1 mutation is a direct cause of the motor neuron disease amyotrophic lateral sclerosis (ALS, or Lou Gehrig's disease), and recent studies also located VCP mutations as a cause of familial and sporadic ALS.[41–43] Oxidative stress and ROS, in addition to presenting as a common risk factor for cancer, and aging diseases of aggregated proteins such as Alzheimer's disease, Parkinson's disease and Huntington's disease are similar to IBMPFD. Pathological and human genetic evidence as well as proteomic insight into this report provide a convergent mechanism for ROS in IBMPFD pathogenesis.

Concluding remarks

On the basis of previous reports and our 2D findings, an extension of the previously summarized VCP-mediated pathogenic pathway is depicted in this study. Mutations of VCP consume a large amount of ATP in the cells. As a result, actin dynamics shuts down to save the available ATP for essential house-keeping tasks. This causes actin aggregation which activates ROS production and triggers apoptosis. Our findings contribute to a new discovery and understanding of the molecular pathways and mechanisms responsible for IBMPFD. Combining both the proteomics

Table 3 List of up-regulated and down-regulated proteins expressed in TER94^{WT} fly strain in comparison to TER94^{R188Q} fly strains

Spot no.	Protein name	M_W	MASCOT score[a]	p*I*	Coverage (%)	Matched peptide sequences
Up-regulated proteins expressed in TER94WT fly strain in comparison to TER94R188Q strains						
A49	Guanine nucleotide-binding protein subunit β-like protein	36 109	115/48	7.14	33	TVEELRPEVVSPTSK; DEDTNYGYPQK
B45	Superoxide dismutase	15 974	104/48	5.67	56	GTVFFEQESSGTPVK; EHGAPVDENR
B51	Pigment cell dehydrogenase reductase	28 455	74/60	8.83	19	LRAAHPTQSVMIIK; AAHPTQSVMIIK
C2	Transitional endoplasmic reticulum ATPase TER94	89 545	127/48	5.21	19	GILMYGPPGTGK; EIDIGIPDATGR
C4	Iron regulatory protein 1B (SD12606p)	99 031	145/60	5.6	17	EEGTPLVLVVGK; VSVSDMPEDFK
C6	Drosocrystallin	55 248	78/60	5.54	13	DSLTGDDKR; LDEQQQQR
C11	Synaptosomal-associated protein 25/GH28821p	23 955	90/48	4.51	29	EAEKNLSGMEK; NGMMAQAGYIGR
C17	Sepia/CG6781-PA (RH04924p).	28 566	141/60	5.58	49	GSPMPDVPEDGILR; MSNGRHLAK
C19	Heat shock protein 23	20 730	72/48	5.55	20	SDTTSVEQETVK; DSPIRTLQQLR
C21	Cofilin/actin-depolymerizing factor homolog/ twinstar protein	17 428	62/48	6.74	19	TTYEEIK; MLYSSSFDALKK
C24	CG10233-PA, isoform A (GH04877p)	23 010	87/60	6.62	27	ADGMKYEGEFR; MAMDDYDDDMSSVGVTTAR
C25	Superoxide dismutase CG8905-PA	24 815	83/66	7.74	31	LIQLAPALR; EIMELHHQK
C37	Thioredoxin reductase 1, mitochondrial OS	65 023	92/48	8.11	20	GLGYEPTVMVR; LYGGSTQRMDYK
C38	Glutamate decarboxylase OS	58 466	104/48	6.07	18	FWFMWKAK; GSMMITYQPLR
	CG9009 CG9009-PA	65 871	124/66	6.82	22	MNPAAQLLRMR; VYASTGVLPASTEAK
C41	T-complex protein 1 subunit alpha OS	60 089	86/48	6.03	16	
C44	CG32029-PA (RE57183p)	30 860	70/60	5.97	22	GSYSVVDSDGFIR; GSYSVVDSDGFIRTVK
C47	GTP cyclohydrolase 1	35 804	66/48	6.16	16	AAKAMLYFTK; TVTSTMLGVFR
C48	GTP cyclohydrolase 1	35 804	72/48	6.16	16	TVTSTMLGVFR; EALLPDMAR
C51	Cuticular protein 72Ec CG4784-PA	50 593	87/66	5.4	14	QISSDRDGDDLR; AELSAMLADR
C52	Cuticular protein 72Ec CG4784-PA	50 593	90/60	5.4	19	QISSDRDGDDLR; QDLRIDQESR
29	Guanine nucleotide-binding protein subunit β-2	39 109	82/48	6.3	23	LYDEINGMIQK; MPKIDPETQK

Spot no.	Protein name	M_W	MASCOT score[a]	p*I*	Coverage (%)	Matched peptide sequences
Down-regulated proteins expressed in TER94WT fly strain in comparison to TER94R188Q strains						
B17	Transferrin precursor/ Transferrin CG6186-PA	72 963	168/60	6.89	24	NVGYKIPITK; SDTTSVEQETVK
B19	Transferrin CG6186-PA	72 964	145/60	6.69	22	VSSSDDGEVQIVPASELEK; FFANGLQAQNK
C1	Transitional endoplasmic reticulum ATPase TER94	89 545	144/48	5.21	22	EKMDLIDLEDDK; IVSQLLTLMDGMK
C3	Iron regulatory protein 1B (SD12606p)	99 031	137/60	5.6	15	EEGTPLVLVVGK; RPPFFEGMTR
C18	Triosephosphate isomerase	26 894	76/48	6	26	GAFTGEISPAMLK; QWLSDNISK
C31	Guanine nucleotide-binding protein subunit beta-2	39 109	74/48	6.3	16	LYDEINGMIQK; LWDVREEGHK
C33	Arginine kinase	40 126	193/48	6.04	45	EMYDGITELIK; GKFYPLTGMEK
C34	Isocitrate dehydrogenase CG7176-PA, isoform A	47 030	90/60	6.29	22	LIDDMVAYAMK; MWKSPNGTIR
C40	Glutamate decarboxylase OS	58 466	115/48	6.07	18	FWFMWKAK; GSMMITYQPLR
C53	Aldehyde dehydrogenase CG3752-PA	57 325	70/66	6.37	9	EEIFGPVQQLIR; TIPMDGDFFTYTR

[a] The scores means ($-10\text{Log}(P)$, where P is the probability/threshold score with p-value = 0.05). Identified proteins with a score, $-10\text{Log}(P)$, greater than threshold scores demonstrate the identification of this protein is significant ($p < 0.05$).

approach and fruit fly genetics helps to define the molecular pathways that underlie the process of IBMPFD. This in turn is likely to substantially lead to better understanding of the multi-degenerative IBMPFD pathogenesis and provide new therapeutic targets.

Abbreviations

2D-DIGE two-dimensional difference gel electrophoresis
AAA ATPases associated with a variety of activities
CHAPS 3-[(3-cholamidopropyl)-dimethylammonio]-1-propanesulfonate)
HCCA α-cyano-4-hydroxycinnamic acid
DIGE differential gel electrophoresis
DTT dithiothreitol
FTD frontotemporal dementia
IAM iodoacetamide
IBMPFD inclusion body myopathy associated with Paget's disease of the bone and frontotemporal dementia
MALDI-TOF matrix assisted laser desorption ionization-time of flight
PDB Paget's disease of bone
PTM post-translational modification
ROS reactive oxygen species
SOD superoxide dismutase
TER94 transitional endoplasmic reticulum ATPase
TFA trifluoroacetic acid
UAS upstream activating sequence
VCP valosin-containing protein

Declaration of competing interests

The authors confirm that there are no conflicts of interest.

Table 4 List of up-regulated and down-regulated proteins expressed in TER94^{WT} fly strain in comparison to TER94^{R152H} fly strains

Spot no.	Protein name	M_W	MASCOT score[a]	p*I*	Coverage (%)	Matched peptide sequences
Up-regulated proteins expressed in TER94WT fly strain in comparison to TER94R152H fly strains						
D7	Iron regulatory protein 1B	99 031	103/60	5.6	13	EEGTPLVLVVGK; VSVSDMPEDFK
D31	Arginine kinase	40 126	130/48	6.04	29	GKFYPLTGMEK; EMYDGITELIKLEK
D43	CG12079-PA (RH59487p) (LD25561p).-	30 181	105/60	7.7	29	MASTTPVEPK; FDLSAPWEQFPNFR
18	Triosephosphate isomerase	26 894	76/48	6	26	QWLSDNISK; MNGDQKSIAEIAK
Spot no.	Protein name	M_W	MASCOT score[a]	p*I*	Coverage (%)	Matched peptide sequences
Down-regulated proteins expressed in TER94WT fly strain in comparison to TER94R152H strains						
D6	Iron regulatory protein 1B	99 031	90/60	5.6	10	EEGTPLVLVVGK; RPPFFEGMTR
D8	Acetyl-coenzyme A synthetase	76 709	87/48	5.47	11	YWSVIDK; VEEMGHSVEK
D15	Glutamine synthetase 2 cytoplasmic	41 962	87/48	5.42	23	TLDFIPQSPK; MSARILEDSPNAR
D18	AE003796	55 031	92/60	5.71	18	YSLIHAHR; ALINLDSAGSGGR
D19	NADH-ubiquinone reductase 75 kDa subunit	56 273	71/60	6.3	13	FTDINYTGK; TSAMVAQTPAK
D26	Glutamate decarboxylase	58 466	97/48	6.07	19	FWFMWKAK; IATNEVGKMR
D29	Isocitrate dehydrogenase CG7176-PC, isoform C	52 955	164/60	7.16	31	TAAMMTSVHR; MSAVSEMAQK
D33	Probable isocitrate dehydrogenase [NAD] subunit alpha, mitochondrial; lethal (1) G0156 CG12233-PB, isoform B	41 160	118/48	6.96	25	TLYDDVDVVTIR; IGLKGPLMTPVGK
37	Thioredoxin reductase 1, mitochondrial OS	65 023	92/48	8.11	20	GLGYEPTVMVR; LYGGSTQRMDYK

[a] The scores means ($-10\mathrm{Log}(P)$, where P is the probability/threshold score with p-value = 0.05). Identified proteins with a score, $-10\mathrm{Log}(P)$, greater than threshold scores demonstrate the identification of this protein is significant ($p < 0.05$).

Acknowledgements

This work was supported by NTHU Booster grant and Nano- and Micro- ElectroMechanical Systems-based Frontier Research on Cancer Mechanism, Diagnosis, and Treatment grant from National Tsing Hua University. The authors also appreciate the kind provision of different fly strains from Brain Research Center and Prof. Ann-Shyn Chiang's laboratory in National Tsing Hua University, Taiwan. We also thank Prof. Ann-Shyn Chiang for discussion and comments on the manuscript.

References

1 V. E. Kimonis, E. Fulchiero, J. Vesa and G. Watts, *Biochim. Biophys. Acta*, 2008, **1782**, 744–748.
2 V. E. Kimonis, S. G. Mehta, E. C. Fulchiero, D. Thomasova, M. Pasquali, K. Boycott, E. G. Neilan, A. Kartashov, M. S. Forman, S. Tucker, K. Kimonis, S. Mumm, M. P. Whyte, C. D. Smith and G. D. Watts, *Am. J. Med. Genet., Part A*, 2008, **146**, 745–757.
3 G. D. Watts, J. Wymer, M. J. Kovach, S. G. Mehta, S. Mumm, D. Darvish, A. Pestronk, M. P. Whyte and V. E. Kimonis, *Nat. Genet.*, 2004, **36**, 377–381.
4 C. C. Weihl, A. Pestronk and V. E. Kimonis, *Neuromuscular Disord.*, 2009, **19**, 308–315.
5 M. J. Kovach, B. Waggoner, S. M. Leal, D. Gelber, R. Khardori, M. A. Levenstien, C. A. Shanks, G. Gregg, M. T. Al-Lozi, T. Miller, W. Rakowicz, G. Lopate, J. Florence, G. Glosser, Z. Simmons, J. C. Morris, M. P. Whyte, A. Pestronk and V. E. Kimonis, *Mol. Genet. Metab.*, 2001, **74**, 458–475.
6 C. U. Hubbers, C. S. Clemen, K. Kesper, A. Boddrich, A. Hofmann, O. Kamarainen, K. Tolksdorf, M. Stumpf, J. Reichelt, U. Roth, S. Krause, G. Watts, V. Kimonis, M. P. Wattjes, J. Reimann, D. R. Thal, K. Biermann, B. O. Evert, H. Lochmuller, E. E. Wanker, B. G. Schoser, A. A. Noegel and R. Schroder, *Brain*, 2007, **130**, 381–393.
7 M. H. Helfrich and L. J. Hocking, *Arch. Biochem. Biophys.*, 2008, **473**, 172–182.
8 S. H. Ralston, *Bone*, 2008, **43**, 819–825.
9 J. B. Guinto, G. P. Ritson, J. P. Taylor and M. S. Forman, *Acta Neuropathol.*, 2007, **114**, 55–61.
10 R. M. Liscic, *Arh. Hig. Rada Toksikol.*, 2009, **60**, 117–122.
11 I. T. Pleasure and M. M. Black, *et al.*, *Nature*, 1993, **365**(6445), 459–462.
12 M. Egerton, O. R. Ashe, D. Chen, B. J. Druker, W. H. Burgess and L. E. Samelson, *EMBO J.*, 1992, **11**, 3533–3540.
13 S. Jentsch and S. Rumpf, *Trends Biochem. Sci.*, 2007, **32**, 6–11.
14 C. Mori-Konya, N. Kato, R. Maeda, K. Yasuda, N. Higashimae, M. Noguchi, M. Koike, Y. Kimura, H. Ohizumi, S. Hori and A. Kakizuka, *Genes Cells*, 2009, **14**, 483–497.
15 T. Huyton, V. E. Pye, L. C. Briggs, T. C. Flynn, F. Beuron, H. Kondo, J. Ma, X. Zhang and P. S. Freemont, *J. Struct. Biol.*, 2003, **144**, 337–348.
16 Q. Wang, C. Song, X. Yang and C. C. Li, *J. Biol. Chem.*, 2003, **278**, 32784–32793.
17 Q. Wang, C. Song and C. C. Li, *J. Struct. Biol.*, 2004, **146**, 44–57.
18 B. DeLaBarre and A. T. Brunger, *Nat. Struct. Biol.*, 2003, **10**, 856–863.
19 K. U. Frohlich, H. W. Fries, M. Rudiger, R. Erdmann, D. Botstein and D. Mecke, *J. Cell Biol.*, 1991, **114**, 443–453.
20 V. Pamnani, T. Tamura, A. Lupas, J. Peters, Z. Cejka, W. Ashraf and W. Baumeister, *FEBS Lett.*, 1997, **404**, 263–268.
21 M. Mutsuddi and J. R. Nambu, *Curr. Biol.*, 1998, **8**, R809–R811.
22 A. M. Celotto and M. J. Palladino, *Mol. Interventions*, 2005, **5**, 292–303.
23 Y. C. Chang, W. T. Hung, H. C. Chang, C. L. Wu, A. S. Chiang, G. R. Jackson and T. K. Sang, *PLoS Genet.*, 2011, **7**, e1001288.
24 C. Ericsson, *Methods Mol. Biol.*, 1999, **112**, 35–41.
25 H. N. Shah, C. J. Keys, O. Schmid and S. E. Gharbia, *Clin. Infect. Dis.*, 2002, **35**, S58–S64.
26 H. L. Chan, S. Gharbi, P. R. Gaffney, R. Cramer, M. D. Waterfield and J. F. Timms, *Proteomics*, 2005, **5**, 2908–2926.
27 D. Halawani, A. C. LeBlanc, I. Rouiller, S. W. Michnick, M. J. Servant and M. Latterich, *Mol. Cell. Biol.*, 2009, **29**, 4484–4494.
28 X. Li, C. Standley, E. Sapp, A. Valencia, Z. H. Qin, K. B. Kegel, J. Yoder, L. A. Comer-Tierney, M. Esteves, K. Chase, J. Alexander, N. Masso, L. Sobin, K. Bellve, R. Tuft, L. Lifshitz, K. Fogarty, N. Aronin and M. DiFiglia, *Mol. Cell. Biol.*, 2009, **29**, 6106–6116.
29 J. R. Bamburg and O. P. Wiggan, *Trends Cell Biol.*, 2002, **12**, 598–605.
30 B. W. Bernstein and J. R. Bamburg, *J. Neurosci.*, 2003, **23**, 1–6.
31 S. J. Atkinson, M. A. Hosford and B. A. Molitoris, *J. Biol. Chem.*, 2004, **279**, 5194–5199.

32 C. W. Gourlay and K. R. Ayscough, *Biochem. Soc. Trans.*, 2005, **33**, 1260–1264.
33 C. W. Gourlay and K. R. Ayscough, *FEMS Yeast Res.*, 2005, **5**, 1193–1198.
34 C. W. Gourlay and K. R. Ayscough, *Nat. Rev. Mol. Cell Biol.*, 2005, **6**, 583–589.
35 C. W. Gourlay and K. R. Ayscough, *J. Cell Sci.*, 2005, **118**, 2119–2132.
36 C. W. Gourlay, L. N. Carpp, P. Timpson, S. J. Winder and K. R. Ayscough, *J. Cell Biol.*, 2004, **164**, 803–809.
37 M. Breitenbach, P. Laun and M. Gimona, *Trends Cell Biol.*, 2005, **15**, 637–639.
38 T. Eisenberg, S. Buttner, G. Kroemer and F. Madeo, *Apoptosis*, 2007, **12**, 1011–1023.
39 A. Griciuc, L. Aron, M. J. Roux, R. Klein, A. Giangrande and M. Ueffing, *PLoS Genet.*, 2010, **6**, e1001075.
40 M. Ueffing, *J. Biol. Chem.*, 2006, **281**, 25757–25767.
41 C. E. Shaw, *Neuron*, 2010, **68**, 812–814.
42 M. Dejesus-Hernandez, P. Desaro, A. Johnston, O. A. Ross, Z. K. Wszolek, N. Ertekin-Taner, N. R. Graff-Radford, R. Rademakers and K. Boylan, *Neurology*, 2011, **77**, 1102–1103.
43 R. J. Braun and H. Zischka, *Biochim. Biophys. Acta*, 2008, **1783**, 1418–1435.